千葉大学審査学位論文（要約）（Summary）

大学院融合科学研究科　　情報科学専攻
Graduate School of Advanced Integration Science　　Information Science Division

知能情報コース

Information Processing and Computer Science Department

学生証番号 16YD1301
Student ID Number

氏　名 RAZI Pakhrur
Name

論文題名（外国語の場合は、その和訳を併記）

Thesis Title（foreign language title must be accompanied by Japanese translation）

Analysis of Land Deformation using Persistent Scatterer Interferometry and Quasi Persistent Scatterer Techniques

(永久散乱体による干渉法と疑似永久散乱体法を用いた地殻変動の解析)

Analysis of Land Deformation using Persistent Scatterer Interferometry and Quasi Persistent Scatterer Techniques

THESIS SUMMARY

Abstract

Complex topography and geological formation are the primary causes of frequent land deformation occurrence at Kelok Sembilan area, West Sumatra, Indonesia. In this research, land deformation monitoring was carried out at Kelok Sembilan area using Persistent Scatterer Interferometry (PSI) and Quasi-Persistent Scatterer (Q-PS) Interferometry technique based on synthetic aperture radar (SAR). The PSI technique was employed to process 13 scenes of L-band SAR data from a satellite (ALOS PALSAR) that were recorded from July 2007 to November 2010. The land deformation analysis was performed in two of the critical landslide areas near the Kelok Sembilan flyover. The research also employed the Q-PS technique to analyze 90 scenes of C Band SAR onboard Sentinel-1A satellite that was observed from October 2014 to November 2017 with VV and VH polarizations. The Q-PS technique was used to improve the spatial distribution of persistent scatterer (PS) points available for Sentinel-1A satellite data that are characterized by shorter wavelength and low resolution than ALOS PALSAR data. Furthermore, the research also investigated the PS point distribution and density in V-contour-shaped terrains due to the azimuthal slope effect for both VV and VH polarizations. The results of PSI and Q-PS analysis were validated using the positional data from differential global positioning system (DGPS) technique as well as 3D ortho-photographs collected by an Unmanned Aerial Vehicle (UAV) and processed by 3D photogrammetry technique. These ground survey results indicated the accuracy of the PSI and Q-PS methods applied to the SAR data analysis. Thus, this research, as a whole, has succeeded in mapping the landslide distributions, contributing to future disaster prevention and mitigation in the study area.

1. Introduction

1.1 Background

West Sumatera lies in the megathrust subduction zone where two tectonic plates collide each other. Indo-Australia plate is pushed down to Eurasia plate where Sumatera island is on top of Eurasia plate. This movement causes earthquakes which often have high magnitude [1]. Therefore it causes deformation on earth surface (uplift/subsidence). Also, there are Mentawai, and Sumatera fault zones span from Lampung to Aceh, where the path of the fault divides the area of West Sumatera into two regions. Consequently, the tectonic earthquake in October 2009 not only ruined many buildings but also caused landslide in many places in West Sumatera. Landslide in Gunung Tigo Padang Pariaman caused by the earthquake, for instance, has piled up two villages (Cumanik and Lubuk Laweh) and all of the inhabitants [2]. Also, West Sumatera has a hilly surface with a very high annual rainfall intensity. Therefore, many places are susceptible to landslide. The most area with landslide susceptible is in transportation pathway of West Sumatera province–Riau province along. There were three large landslide occurrences in the last three years, 35 landslide points in 2015, 50 landslide points in 2016, and 64 landslide points in 2017 [3]. The landslide inhibits transportation and economic growth of both provinces.

The monitoring of land deformation on the research study is carried out by two techniques and two different sources of satellite SAR data. First, the Persistent Scatterer Interferometry (PSI) Synthetic Aperture Radar (SAR) technique. It is a sophisticated technique for monitoring and detecting land deformation on the earth surface that can overcome the geometric and temporal decorrelation [4]-[5], and atmospheric disturbance in comparison to conventional interferometry. As a result, the accuracy of the technique can be achieved in millimeter order [6]. The data used Advanced Land Observing Satellite Phased Array Type L-band Synthetic Aperture Radar (ALOS PALSAR) which provided by Japan Aerospace Exploration Agency (JAXA). This satellite uses active microwave sensor at the frequency of 1270 MHz (L-band) which has many advantages, such as the ability to observe earth surface even in cloudy

condition during the day and the night [7]. This satellite with L-band operating frequency is used as it can penetrate up to the land surface [8]. Therefore it is appropriate to detect landslide even in the forest [9]. ALOS PALSAR has a high resolution of 10 m with a wide observation area around 40-70 km for fine mode and 250-350 km for scanSAR mode, with 46 days revisited time [10]. The satellite is operable for full observation in Asia. Therefore, it is appropriate for PSI method which requires many SAR images. Second, the Quasi-Persistent Scatterer (Q-PS) technique. The technique used to improve the persistent scatterer (PS) point on the spatial distribution. It is required because the satellite data was applied has a short wavelength (C-band), and low coherence due to the local steep slope and vegetation on the area of research. The interferometry SAR data of Sentinel-1A which provided by the European Space Agency (ESA) has been used. This data was selected because Sentinel-1A (C-band) SAR images have a small perpendicular baseline B_n (about 200 m) as well as the temporal baseline B_t (12 days), then, it can reduce the geometric and temporal decorrelations in SAR processing. Consequently, using this data can improve the accuracy of measurement.

The application of the PSI technique for monitoring land deformation over the area using ALOS PALSAR (L-band) with linear cross-polarization HV (Horizontal transmit, Vertical receive) is limited to ascending orbit direction. In Q-PS technique, in addition to continuous inspection on the area, an investigation of land deformation is also performed using short wavelength (C-band) for both sides of the field with 'V' contour shape from ascending and descending orbits. Also, investigate the PS point distributions and density due to the terrain slope effect [11],[12] for linear co-polarization (VV) and cross-polarization (VH) that related to the consistency of land deformation detection.

The result from PSI and Q-PS techniques analysis ware validate with *in-situ* ground truth survey and measurement recorded using Geodetic GPS with differential GPS technique and 3D orthophoto that synthesis using the 3D photogrammetry technique. Also, clinometer and measuring tape were used to measure the tilt and unsymmetrical properties of the bridge

1.2 Research Objectives

The objectives of this research are to measure and analyze the land deformation using the PSI technique and Q-PS technique.

2. Study Area and Satellite Dataset

The area of research located in the Kelok Sembilan flyover at a latitude and longitude of 0° 4' 13.30" S and 100° 41' 53.56" E, respectively. The area is part of Lima puluh Kota district, West Sumatra, Indonesia. The area is hilly that has a long time recorded the land deformations [13]. Kelok Sembilan flyover is the main road connecting both West Sumatra province and Riau Province. The flyover was built to reduce the traffic loads due to the slope of the old roads. The flyover construction designed meandering in the center of two hilly mountainous zones

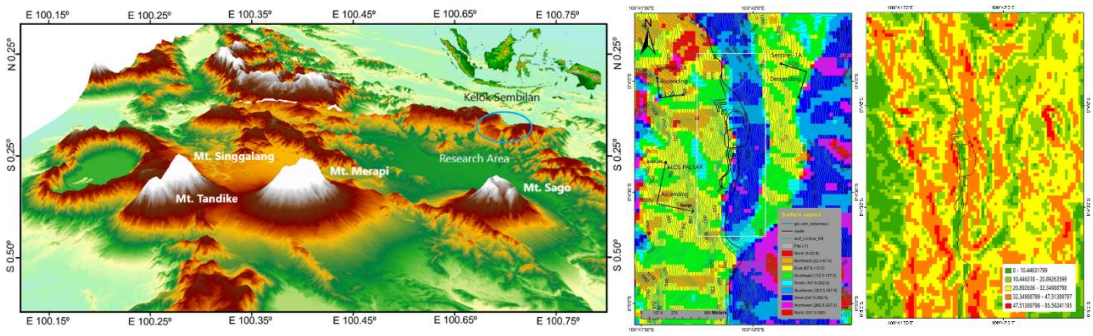

Figure 2. 1 (Left): The topography of West Sumatra based on Shuttle Radar Topography Mission (SRTM) Digital Elevation Model (DEM) with 30 m resolution. (Center): Geomorphology structure and topography of Kelok Sembilan region. (Right): Slope Kelok Sembilan Area extracted from Digital Elevation Model 12 m Resolution

The satellite data used for PSI and Q-PS technique is listed on Table 2.1

Table 2.1 Satellite dataset for PSI and Q-PS technique, respectively.

No	Acquisition Date (DD/MM/YYYY)	Mode	Normal Baseline B_n (m)	Temporal baseline B_t (Days)	Off Nadir Angle
1	03072007	FBD	74	-460	34.3^0
2	18082007	FBD	-24	-414	34.3^0
3	03102007	FBD	211	-368	34.3^0
4	20052008	FBD	259	-138	34.3^0
5	05072008	FBD	155	-92	34.3^0
6	20082008	FBD	626	-46	34.3^0
7	05102008	FBD	0	0	34.3^0
8	08072009	FBD	758	276	34.3^0
9	08102009	FBD	-134	368	34.3^0
10	11072010	FBD	272	644	34.3^0
11	26082010	FBD	82	690	34.3^0
12	11102010	FBD	120	736	34.3^0
13	26112010	FBD	351	782	34.3^0

No	Orbit	The number of Scenes	Beam swath mode	Acquisition Time	Polarization	Off-Nadir angle
1	Ascending	36	IW 1	10/2014-03/2017	VV+VH	26.00^0-32.48^0
2	Descending	54	IW 3	10/2014-11/2017	VV+VH	35.35^0-40.40^0

3. METHODOLOGY

3.1 Persistent Scatterer Interferometry (PSI) Synthetic Aperture Radar Technique

Persistent Scatterer Interferometry (PSI) technique initially developed by SAR group of Politecnico di Milano (POLIMI) [4],[5]. The main idea of this technique is to detect highly coherent point-like PS target by using amplitude stability as an indicator of phase stability in time series. The analysis result based on a set of radar SAR images in different time acquisition in the same area.

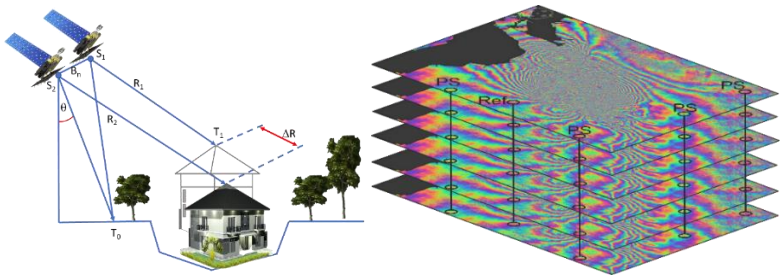

Figure 3. 1 Schematic land deformation detection by identify the coherent radar target. (a). Repeat-pass SAR satellite detection of the land deformation. (b). Satellite data stack of multitemporal SAR acquisition with sparse PS grid.

The SAR images that produce from each satellite observation is stacked with referring to one unique master image and then identify its PS based on the coherent radar target for all satellite data set. Based on the PS candidate (PSC), the atmospheric effect can be estimates and removes. Finally, the velocity and displacement in time series can be obtained. The schematic of PSI processing is depicted in Figure 3.2.

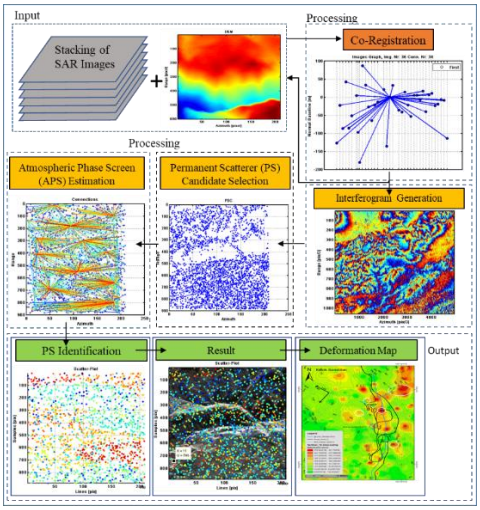

Figure 3.2 Generic flowcharts of PSI technique for land deformation detection

Phase component that contribute in PSI and Q-PS technique are

$$\Delta\phi_{m,s}(T) = \frac{4\pi}{\lambda}\frac{B_n}{R_m}\frac{\Delta h(T)}{sin\theta} + \frac{4\pi}{\lambda}B_t\Delta v(T)$$

The first term of the equation means, the profile of image on the ground is function of the height of the point T and linear with normal baseline. The second term means, the phase movement is function of relative velocity of point T with respect to reference point (linear model)

3.2 Quasi-Persistent Scatterer Technique

3.2.1 Multi-Master Approach

Applying the PSI technique in the non-urban area lead to PS detection is low because the technique only extracted the dominant scatterer. To solve the limitation, new technique requires that can extract the scatterer not only dominant scatterer but also partially coherence targets γ. The technique called as Quasi Persistent Scatterer (Q-PS) that is developed from PSI technique. The idea of Q-PS technique is to enhance the PS point measurement in spatial distribution [14]. Three main points is modified from the original of PSI that used in Q-PS technique [15]: First, the image of the dataset is not required to correlate with one master image (multi-master approach). Second, the height and displacement of a target are estimated by exploiting the coherence interferogram appropriate target. Third, improving the signal-to-noise ratio of the interferometric phase of the extended target by applying the spatial filtering. Q-PS technique is not only proven in an urban area but also in the sub-urban area, which can enhance the density of PSC in spatial distribution [16].

One of some graph configurations in Q-PS technique is Minimum Spanning Tree (MST) with additional coherence parameter as weight used to optimize the coherence value of target γ. The MST graph configuration is searching the minimum best coherent graph connecting for all image dataset. Improving the coherence target, three components of the MST graph configuration are considered. First, the networking of the image, it is required to unwrap the phase in time series. Second, the connectivity number. Third, the weight value to each connectivity in order to determining its quality [15].

3.2.2 Weighted Approach

Additional parameter improvement from original PSI is by introducing weight in parameter estimation. Weight is a parameter that marking which the interferogram that given target is coherent. The weight can be implemented in order to keep the interferometry phase sample in height and velocity estimation.

$$\xi[\Delta v(p), \Delta h(p)] = \frac{1}{\sum w_{m,s}}\sum_{m,s}^{N_{Int}} w_{m,s}\, e^{j[\Delta\phi_{m,s}(p) - k_v\Delta v(p)B_{t,m,s} - k_h\Delta h(p)B_{n,m,s}]}$$

Only the interferometric phase with high weight $w_{m,s}$ will be used to estimating the model parameter.

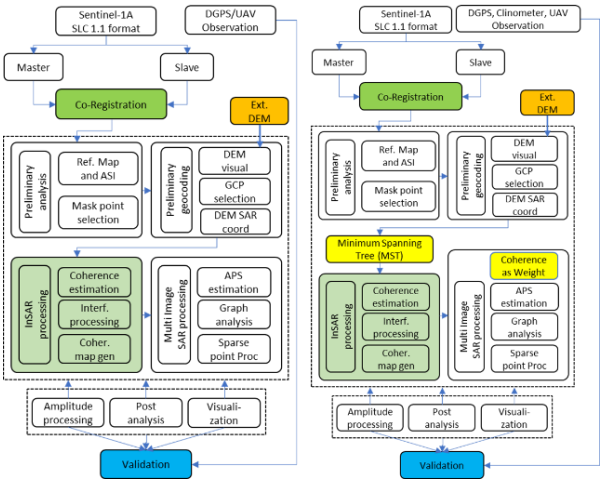

Figure 3.3 Flowchart PSI and Q-PS technique

3.2.3 SAR images selection

The criteria SAR images selection is depending on the specific application of the study area. The main decision is related to the type of sensor, availability of the data, the normal baseline, and temporal baseline, characteristic of terrain and atmospheric condition during image acquisitions time [17]. The important parameter of sensor and satellite that should be considered is wavelength, bandwidth, SNR, orbit inclination and repeat time. Wavelength is ensuring the depth of penetrating electromagnetic wave and its sensitivity to ionosphere and weather condition. Also, the wavelength and SNR combination is impacting the fringe density due to topography condition of the study area. The bandwidth range influenced the image resolution and its critical baseline whereas the orbit inclination of the satellite is to determine the coverage area of the earth and repeat time SAR satellite acquisition.

The other parameter should be a concern is the availability of SAR data included a different view of the satellite from ascending and descending orbit. These are important to reduce the image distortion and to resolve the different component of deformation vectors. For surface deformation, normal baseline minimum is referred to reduce phase signal due to the topography and noise due to the phase gradients. To minimize the temporal decorrelation effect in land mapping, the shortest temporal baseline is possibly used to gain the coherence value [18]

3.2.4 Master Image Selection

The master image is selected base on *maximization stack coherence* value of image combination. In visual can be selecting the center of the normal baseline B_n of all satellite images and acquisition time B_t. The stack coherence γ^m model with master image m is defined as [19]

$$\gamma^m = \frac{1}{N}\sum_{N=1}^{N} g(B_n^{m,s}, B_{n\,max}).\, g(B_t^{m,s}, B_{t\,max}).\, g(B_{DC}^{m,s}, B_{DC\,max})$$

where $g(x,c) = \begin{cases} 1 - \frac{|x|}{c_r} \; if \; |x| < c_r \\ 0 \; otherwise \end{cases}$

The master images selected based on the acquisition time whereas stack coherence γ^m will have larger in centre of time, the centre of normal baseline and doppler centroid as well.

3.2.5 Co-registration

Co-registration is a fundamental step to ensure each ground target has the same range and azimuth pixel between the master and slave images [18]. It is required to able to calculate the interferogram oversampled master and slave because the pixel of both master and slave images must cover the same area on the earth surface. In this step account the orbit crossings, skewing, different sensor attitudes, different sampling rate, and track shift (along and across) [20]. Inaccuracies co-registration influence the decorrelation effect hence produced the noise in phase observation.

3.2.6 Interferogram Generation (optional)

Generating interferogram is formed by cross multiplication the pixel by pixel between a master image with the complex conjugate of slaves. The Digital Elevation Model (DEM) and precise orbit are used to reference the interferogram [19]. Interferometric phase is containing the information about the land deformation, topographic height different, residual orbital error and atmospheric disturbance. The result of PS processing does not depend on the precise of DEM, because the elevation and pixel in each cell respect to DEM are estimated.

3.2.7 Persistent Scatterer Candidate (PSC) selection

The stack of radar interferometry SAR data contains billions of images pixel. Then, the Persistent Scatterer Candidate (PSC) is identified by a statistical analysis using their amplitude value [5] or finding the pixel that has high phase stability (coherence) value in most of the interferogram [4]. In this case, the Amplitude Stability Index (ASI) used to select the PSC. The amplitude stability index is a ratio between the mean and standard deviation of an amplitude value of SAR images that computed on a pixel by pixel basis [21], without spatial smoothing. Also, it has a relation with Amplitude dispersion index (D_a) [5].

$$ASI = 1 - D_a$$

The relation between phase standard deviation σ_φ and D_a is express as $tan\,\sigma_\varphi \cong \frac{\sigma_a}{m_a} \triangleq D_a\,[rad]$. where σ_a is the amplitude standard deviation and m_a is the amplitude mean in time series.

The dispersion index D_a is a measure of phase stability which the better value is for low σ_φ. The amplitude depression value $D_a < 0.25$ were selected as PCS for urban area [5], and $D_a < 0.4$ for non-urban area [22] or $D_a < 0.4$ with minimum PSC density 3 PCS/km2 [23] or ASI > 0.6..

3.2.8 Atmosphere Phase Screen

After PSC is selected, the next step is estimating and removing the atmospheric components on each SAR images in Atmospheric Phase Screen (APS). The Delaunay triangulation network formation algorithms are implemented for connecting each PSC [19]. The network is to ensure the integrity of analysis for all area observation. For analyzing wide-area observation, every close point target (PSC) is connected which referring to the single reference point. More redundancy networks created in this approach, it is useful to reduce the phase ambiguity error and the stability of the network.

3.2.9 Height and Velocity PS Estimation

Estimation height $\Delta h(T)$ and velocity $\Delta v(T)$ for each PS point in space function of normal baseline $B_{n,i}$ and temporal baseline $B_{t,i}$ propose by maximization of the periodogram. The periodogram $\xi[\Delta v(T), \Delta h(T)]$ can be written as [24], [15].

$$\xi[\Delta v(T), \Delta h(T)] = \frac{1}{N_i}\sum_{i=1}^{N_i} e^{j[\Delta\phi_{m,s}(T) - k_v \Delta v(T) B_{t,i} - k_h \Delta h(T) B_{n,i}]}$$

where $k_v = \frac{4\pi}{\lambda}$ and $k_h = \frac{4\pi}{\lambda R \sin\theta}$ is the factor that is linking the velocity to temporal baseline and height to normal baseline, with an assumption the flat terrain component $\Delta\phi_{m,s}(p)$ removed. N_i is a number of the image.

4. RESULT AND DISCUSSION

4.1 Land Deformation Monitoring using PSI Technique

Based on the PS point, there are two areas with high critical land movement. The area called as area 1 and area 2 that located on the positive slope of Kelok Sembilan flyover as shown in Figure 4. 11. In the past time, the landslide incidents ware occurring in both area 1 and 2. The other spot remaining area on the Kelok Sembilan were not included in the analysis due to the limitation of ground truth data and dangerous topography condition. The coherency of PS point on both areas observation is in range of 0.6 to 0.65. The low value of coherency can be used as an indication that the area is moving.

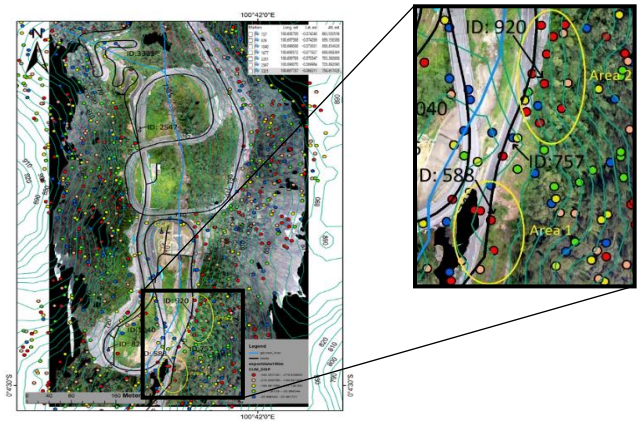

Figure 4. 1 Persistent scatterer point from PSI processing geocoded into 3D orthophoto with WGS-84 coordinate system. The road in Kelok Sembilan was indicated as a black line and Sanipan river is blue line. Two yellow ellipse lines are concern area observation. Insert picture top-right is PS point selected for validation and below-right is cumulative displacement of PS point.

Tracking the history of the land deformation that indicates by PS point in time series presented in Figure 4. 2. One point selected as a representation of land deformation for the area concern. From the analysis, for both PS point ID that represents its area, the acceleration values are -23.06 mm/month^2 and -5.4 mm/month^2, respectively. The value correlates with rainfall intensity. During the time, the raindrop intensity is high, 251 mm/month and 215 mm/month both Area 1 and Area 2, respectively [23].

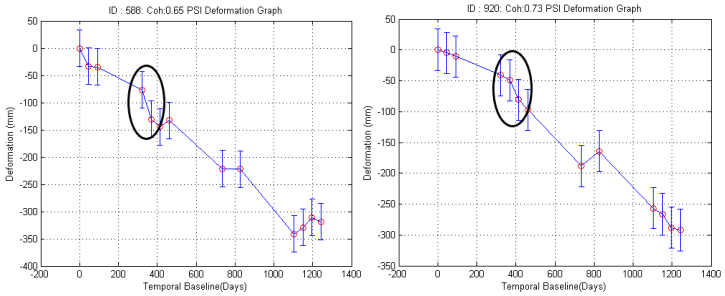

Figure 4. 2 The histories of land deformation that represented by ID 588 and ID 920 for both area 1 and area 2, respectively. Black circles are acquisition time that has a high acceleration of land deformation. The observation was starting from July 2007 to November 2010.

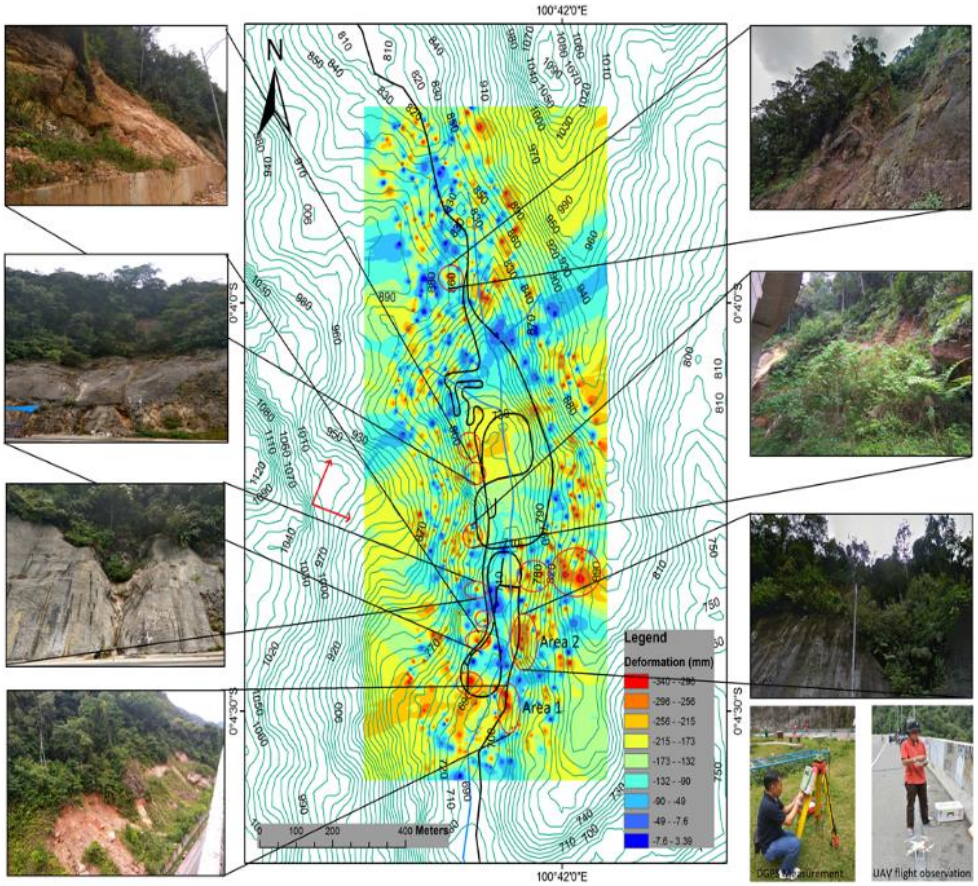

Figure 4. 3 Deformation map of Kelok Sembilan area that projected into the WGS84 coordinate system. The area that has significant land movement indicates as a red circle. Insert image on the right-below deformation movement in millimeter. The picture on the right and left of deformation map is the ground truth observation that associate with significant area movement.

Figure 4. 3 presents the land deformation map that projected into WGS84 coordinate system included with contour shape of Kelok Sembilan area that processes using PSI and geographic Information system (GIS). PS point that produces from PSI processing converted to raster using Inverse Distance Weighted (IDW) technique. The maximum movement of the land in both area 1 and area 2 is -318.6mm and -329 mm, respectively. The significant area of movement was indicated by a red circle that has a maximum displacement of more than 300 mm in four years. The average velocity of land movement is -100 mm/year in the LOS of the satellite. The different color of the land deformation map presents the different movement value of PS points. The PSI processing result was confirmed by a ground survey that shows on the right-side and left-side of Figure 4.3. Consequently, the information is useful for local authority and inhabitant that living on the area for preventing or minimizing land deformation impact in Kelok Sembilan region.

4.1.1 Validation

Validation is required to confirm the result obtained from PSI processing is acceptable. In this case, validation result of processing using PSI technique carried out by comparing with in-situ ground truth survey that collected using both geodetic GPS of Leica GPS 1200 plus and observation using Unmanned Aerial Vehicle (UAV) phantom three professional for the selected point of PS. Both recorded using geodetic GPS, and UAV result was compared with PSI processing that tabulated in Table 4.1 in term of latitude, longitude, and elevation of PS point. It presents that the height difference between techniques is less than 0.3%, with root mean square error of PSI-GPS is 0.97 meter, and PSI-UAV is 1.5 meter. Also, the result visualizes in 3D that presented in Figure 4. 4.

Table 4. 1 Comparing Result Measurement Between PSI-GPS and PSI-UAV Based on the in-situ Ground Truth Measurement.

PS	PSI Technique			GPS Geodetic			UAV			Height Error	
ID	LAT	LON	Height (m)	LAT	LON	Height (m)	LAT	LON	Height (m)	% GPS	%UAV
826	-0.074281	100.69759	687.61	-0.074278	100.697520	688.30	-0.074269	100.697588	689.15	0.10	0.22
1040	-0.073636	100.69809	686.92	-0.073632	100.697960	687.62	-0.073631	100.698068	688.85	0.10	0.28
2547	-0.070005	100.69808	726.72	-0.070009	100.697890	727.71	-0.069984	100.698070	728.89	0.14	0.30
3321	-0.068322	100.69770	758.12	-0.068237	100.697610	760.01	-0.068311	100.697737	758.61	0.25	0.06
757	-0.074240	100.69870	662.41	-0.074060	100.698630	662.72	-0.074240	100.698709	663.93	0.05	0.23
1677 (GCP)	-0.071926	100.69858	687.13	-0.071921	100.698470	687.51	-0.071927	100.698572	688.06	0.06	0.14
								Average Height Error		0.12	0.21

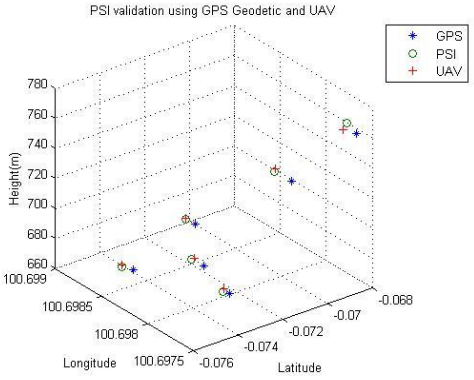

Figure 4. 4 3-Dimensional Visualization of PSI-GPS-UAV measurement for validation the result of PSI processing.

4.2 Land Deformation Monitoring using Quasi-PSI Technique

The Q-PS technique was extracting the information from both ascending and descending orbit of satellite Sentinel-1A in the Kelok Sembilan flyover area. The number of the image was processed in this technique is 36 images and 54 images, respectively. The frequency of the SAR satellite is C-band 5.4 GHz, and wavelength 5.44 cm with wide swath area is 250 km. The data observation was starting from October 10, 2014, to December 7, 2017. Obtaining the consistency information of land deformation in the line of sight, both orbits of the satellite were selected.

The velocity and height are the main component of Q-PS processing that represents the parameter estimation of the land deformation. The land deformation velocities around study area in line and sample for both ascending and descending orbit represented by dots color. The dots color indicates the level of the velocity of the PS point movement. Figure 4. 5 presented the distribution of PS point that represents the deformation of Kelok Sembilan zone extracted using Q-PS processing technique. The polarization of both ascending and descending orbit is VV (vertical transmit and vertical receive). The total number of scenes for both orbits is 90 scenes that taken from October 2014 to March 2017 and October 2014 to November 2017, respectively. The result was geocoded into an optical layer of google earth — the cumulative value of land deformation depicted by RGB dot color of PS point whereas the red color is indicated the highest value of land movement. For both ascending and descending orbit, the maximum movement of the point is -512 mm and -619 mm, respectively.

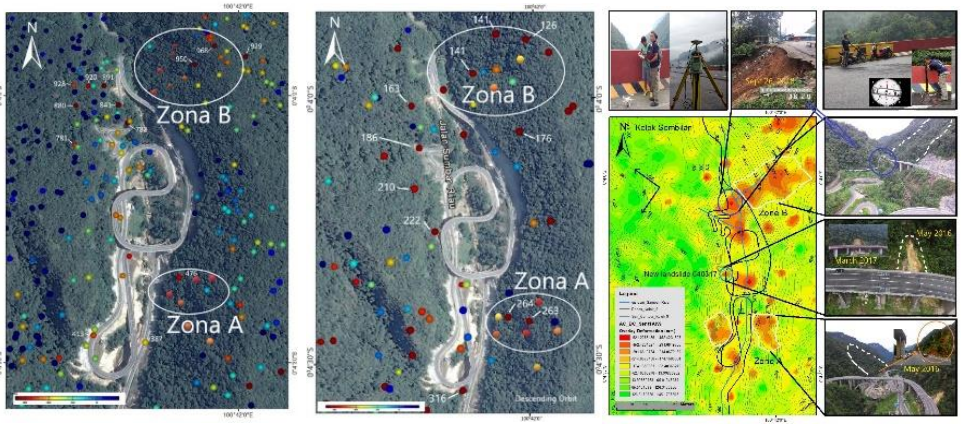

Figure 4. 5 PS point distribution and Map of Land Deformation on Kelok Sembilan area that geocoded into an optical layer of Google Earth and DEM. The point used as an indicator of land deformation. Left: PS point distribution in ascending orbit observed by VV polarization. Center: PS point distribution in descending orbit observed by VV polarization. Right: land deformation mapping. The color of PS point indicates the cumulative value of land deformation. Insert picture in left-below is a color bar of land deformation in millimeter unit.

Figure 4.5 depicts the land deformation area obtained from ascending and descending orbits which were overlaid and modeled based on the Inverse Distance Weighted (IDW) interpolation technique. The technique was selected because it has successfully demonstrated the land movement that also covers small areas. There are six zones of land deformation detection on the positive and negative slopes of Kelok Sembilan bridge. Two of them are critical, namely zone A and zone B that have a significant area covering land deformation with the maximum land movement of more than 500 mm in four years. On the left side of the bridge, the blue cycle shows a landslide area that occurs in May 2016 and March 2017. The last landslide occurred on September 26, 2018, in zone B (opposite to the bridge). In the middle of the valley, some land deformation was also detected which was caused by the construction of the park. Based on ground truth survey observation using UAV, there is a clear distinction of regions that have moved with its surrounding in zone A and zone B.

5. CONCLUSION AND RECOMMENDATION

5.1 Conclusion

The Persistent Scatterer Interferometry (PSI) and Quasi-Persistent Scatterer (Q-PS) technique have proven to be a very effective technique to mapped and monitored the land deformation in Kelok Sembilan flyover in time series. However, in Q-PS technique the PS point is less stable than original PSI because the Q-PS is not only dominant point-like radar target that used to PS point but also distributes scattering. By using the PSI technique, 13 SAR data in ascending orbit captured by the PALSAR sensor of ALOS satellite over four years has successfully extracted for the analysis. From the PSI processing, the main parameter of land deformation such as velocity, displacement, and height was obtained. Based on the result of the analysis, several areas of landslide were successfully identified. Furthermore, for better visualization result, the land deformation contour map was geocoded and overlaid by the 3D photogrammetry of the area of research.

The Q-PS technique is not much different from the PSI technique. The technique also has successfully extracted the C band SAR data of Sentinel-1A for detecting the land deformation. Analyzing the result of processing was supported by ninety scenes of Sentinel-1A for both ascending and descending orbits directions in four years. Furthermore, the PS point obtained from both technique at Kelok Sembilan area was modeled in contour shape by using IDW interpolation technique and projected into Digital Elevation Model (DEM) in 12-meter resolution. From the analysis, two of several land deformation areas with large-scale coverage

were successfully identified by a cumulative displacement that is more than 500 mm and velocity 120 mm/year.

The result from both techniques was validated using the data collected from in situ ground truth measurement recorded using Geodetic GPS LEICA 1200 plus instruments, 3D photogrammetry technique, Clinometer, and measuring tape. Thus, it can be concluded that 1). PSI and Q-PS techniques have the ability to map and monitor land deformation, 2). The one alternative validation tool for the precision of the ground survey is UAV-based 3D photogrammetry.

5.2 Recommendation and Future Research

Monitoring the land deformation using both PSI and Q-PS technique is required a large number of SAR images. Availability of High-resolution SAR images observation in Indonesia besides limited number also expensive, for example, ALOS-2 (L-band) SAR every year only four scenes provided in the most area of Indonesia with same mode and orbit, TerraSAR-X is more less. Only Sentinel-1A/1B with C-band that can support the PSI and Q-PS technique for processing land deformation. Therefore, development SAR system to provide the SAR images is required. In future, besides working on the SAR application, starting research in development SAR system is a big idea to ensure the availability of SAR images with high resolution and low-cost.

References

[1] USGS, "Earthquake Hazards Program," *2017*. [Online]. Available: https://earthquake.usgs.gov/.

[2] PUSDATIN, "Tiga Dusun Dijadikan Kuburan Massal," 2009. [Online]. Available: http://www.kemendagri.go.id/news/2009/10/05/tiga-dusun-dijadikan-kuburan-massal.

[3] BNPB, "Infografis Bencana Banjir & Longsor di Kab. Limapuluh Kota, Sumatera Barat," 2017. [Online]. Available: http://geospasial.bnpb.go.id/2017/03/08/infografis-bencana-banjir-longsor-di-kab-limapuluh-kota-sumatera-barat/.

[4] A. Ferretti, C. Prati, and F. Rocca, "Nonlinear subsidence rate estimation using permanent scatterers in differential SAR interferometry," *IEEE Trans. Geosci. Remote Sens.*, vol. 38, no. 5, pp. 2202–2212, 2000.

[5] A. Ferretti, C. Prati, and F. Rocca, "Permanent Scatters in SAR Interferometry," *IEEE Trans. Geosci. Remote Sens.*, vol. 39, no. 1, pp. 8–20, 2001.

[6] P. Iahs, A. Ferretti, D. Colombo, A. Fumagalli, F. Novali, and A. Rucci, "InSAR data for monitoring land subsidence : time to think big," pp. 331–334, 2015.

[7] JAXA, "Advanced Land Observing Satellite-2 'DAICHI-2' (ALOS-2)," 2017. [Online]. Available: http://global.jaxa.jp/projects/sat/alos2/.

[8] J. T. Sri Sumantyo, M. Shimada, P. P. Mathieu, and H. Z. Abidin, "Long-term consecutive DInSAR for volume change estimation of Land deformation," *IEEE Trans. Geosci. Remote Sens.*, vol. 50, no. 1, pp. 259–270, 2012.

[9] P. Razi, J. T. S. Sumantyo, D. Perissin, and A. Munir, "Persistent Scattering Interferometry SAR based Velocity and Acceleration Analysis of Land Deformation: Case Study on Kelok Sembilan Bridge," in *in Proceedings of 11th International Conference on Telecommunication, Systems, Services, and Applications (TSSA), Lombok,Indonesia*, 2017, pp. 9–12.

[10] JAXA, "ALOS-2 Project / ALOS-2 Overview," 2014. [Online]. Available: http://www.eorc.jaxa.jp/ALOS-2/en/about/overview.htm.

[11] J. Lee, D. L. Schuler, T. L. Ainsworth, E. Krogager, D. Kasilingam, and W. Boerner, "On the Estimation of Radar Polarization Orientation Shifts Induced by Terrain Slopes," vol. 40, no. 1, pp. 30–41, 2002.

[12] D. L. Schuler, J. Lee, T. L. Ainsworth, and R. S. Division, "Correction for Terrain Azimuthal Slope Effects in Polarimetric," no. 202, pp. 1304–1306, 2000.

[13] BNPB, "Data and Disaster Information of Indonesia," *http://dibi.bnpb.go.id*, 2017. [Online]. Available: http://dibi.bnpb.go.id/data-bencana/lihat-data.

[14] D. Perissin and W. Teng, "Repeat-Pass SAR Interferometry With Partially Coherent Targets," *Geosci. Remote Sensing, IEEE Trans.*, vol. 50, no. 1, pp. 271–280, 2012.

[15] D. Perissin and T. Wang, "Repeat-pass SAR interferometry with partially coherent targets," *IEEE Trans. Geosci. Remote Sens.*, vol. 50, no. 1, pp. 271–280, 2012.

[16] D. Perissin and T. Wang, "Time-series InSAR applications over urban areas in China," *IEEE J. Sel. Top. Appl. Earth Obs. Remote Sens.*, vol. 4, no. 1, pp. 92–100, 2011.

[17] R. F. Hanssen, *Radar Interferometry - Data Interpretation and Error Analysis*, vol. 2, no. 8. 2001.

[18] A. Ferretti, A. Monti-Guarnieri, C. Prati, and F. Rocca, *InSAR Principles: Guidelines for SAR Interferometry Processing and Interpretation. Tech.Rep.TM-19, Feb. 2007*. The Netherlands: ESA Publications, 2007.

[19] B. M. Kampes, *Radar Interferometry*, vol. 12. The Netherlands: Springer, 2006.

[20] A. Ferretti, A. Monti-Guarnieri, C. Prati, and F. Rocca, "InSAR processing: a practical approach," in *ESA Publications*, vol. B, 2007, pp. 1–40.

[21] A. Ferretti, *Satellite InSAR Data Reservoir Monitoring from Space*. Netherlands: EAGE, 2014.

[22] A. Ferretti and F. Rocca, "Analysis of Permanent Scatterers in SAR interferometry Analysis of Permanent Scatterers in SAR Interferometry," in *Geoscience and Remote Sensing Symposium, 2000. Proceedings*, 2000, no. February, pp. 761–763.

[23] C. Colesanti, A. Ferretti, R. Locatelli, G. Savio, I. T. E. T. R. E. S, and V. V Colonna, "Multi-platform Permanent Scatterers Analysis : First Results," pp. 52–56.

[24] D. Perissin, "Interferometric SAR Multitemporal Processing : Techniques and Applications," in *Multitemporal Remote Sensing, Remote Sensing and Digital Image Processing*, no. 20, Springer, Cham, 2016, pp. 145–176.